AJNR

Assessment of Diagnostic Accuracy of Perfusion MR Imaging in Primary and Metastatic Solitary Malignant Brain Tumors

Nail Bulakbasi, Murat Kocaoglu, Anar Farzaliyev, Cem Tayfun, Taner Ucoz and Ibrahim Somuncu

AJNR Am J Neuroradiol 2005, 26 (9) 2187-2199
http://www.ajnr.org/content/26/9/2187

Assessment of Diagnostic Accuracy of Perfusion MR Imaging in Primary and Metastatic Solitary Malignant Brain Tumors

Nail Bulakbasi, Murat Kocaoglu, Anar Farzaliyev, Cem Tayfun, Taner Ucoz, and Ibrahim Somuncu

PURPOSE: **The purpose of this study was to estimate the diagnostic accuracy of relative cerebral blood volume (rCBV) measurement in preoperative grading and differentiation of solitary intra-axial malignant brain tumors.**

METHODS: **Thirty-six low-grade glial tumors (LGGTs), 22 high-grade glial tumors (HGGTs), and 17 metastases (METs) were prospectively evaluated by MR imaging and standard dynamic susceptibility contrast-enhanced gradient echo, echoplanar imaging during first pass of a bolus injection of contrast material. Normalized rCBV values from tumoral ($rCBV_T$) and peritumoral ($rCBV_P$) areas were calculated by standard software and statistically tested independently.**

RESULTS: **The mean differences of $rCBV_T$ and $rCBV_P$ values between LGGT (2.30 ± 1.12 and 1.18 ± 0.24) and HGGT (5.42 ± 1.52 and 2.17 ± 0.82) ($P < .001$); HGGTs and METs (3.21 ± 0.98 and 0.97 ± 0.09) ($P < .001$); and LGGTs and METs ($P < .05$ and $P < .001$, respectively) were significant. No clear cutoff value was present. A clear $rCBV_T$ cutoff value of 2.6 was detected for differentiation of low- (1.75 ± 0.38; LGA) versus high-grade (4.78 ± 0.99; HGA) astrocytomas when nonastrocytic glial tumors were excluded. The $rCBV_T$ values were linearly correlated with degree of malignancy ($r = 0.869$; $P < .001$). Cutoff $rCBV_P$ values of 1.1 and 1.2 were quite effective in differentiation of METs from LGGTs and HGGTs, respectively. The overall efficacy of rCBV was higher in grading than in differentiation.**

CONCLUSION: **The diagnostic accuracy of rCBV measurement is higher in grading of glial brain tumors than in differentiation of HGGTs from solitary intra-axial METs. The astrocytic and nonastrocytic glial tumors have to be evaluated separately for precise grading.**

The most frequently encountered challenge in brain tumor diagnosis is the differential diagnosis of a solitary intra-axial brain tumor. It is always problematic to judge whether a tumor is benign or malignant, primary or metastatic, and low or high grade. Despite some characteristic MR imaging findings, it can be difficult, sometimes even impossible, to distinguish between these tumors, and, in such cases, gross tumor resection or stereotactic biopsy is required for precise diagnosis. Another problematic issue is preoperative grading of glial tumors by noninvasive techniques. Dynamic susceptibility contrast-enhanced (DSC) perfusion imaging has long been used to overcome these problems in brain tumors (1–7). As reported elsewhere (4), the results in most of these studies concerning the relationship between relative cerebral blood volume (rCBV) and glial tumor grade or different tumor types have been obtained by experienced radiologists working in a research environment on selected predefined disease entities, usually by using home-made software for postprocessing of raw perfusion data. In this study, all perfusion data were obtained during our routine clinical work and the raw data were postprocessed by standard software developed by the vendor.

Malignant gliomas are among the most vascularized tumors in humans (8). Angiogenesis has a key role in both the growth and malignant transformation of brain tumors; therefore, antiangiogenic treatment strategies have proliferated during the past decade (8–11). Monitoring of such treatment protocols requires in vivo quantitative assessment of tumoral vascularization by means of noninvasive techniques such as DSC perfusion imaging (11). The enhancement

Received March 1, 2005; accepted after revision April 20.

From the Department of Radiology, Gulhane Military Medical School, Ankara, Turkey.

Address correspondence to Nail Bulakbasi, MD, Department of Radiology, Gulhane Military Medical Academy, Etlik, 06018 Ankara, Turkey.

pattern of a tumor on conventional MR imaging is not always reliable to obtain precise information about tumor angiogenesis at the capillary level, because tumoral enhancement is mainly due to the disruption of blood-brain barrier (BBB) rather than the tumoral vascular proliferation itself (12, 13). The DSC perfusion imaging has the potential to provide noninvasive assessment of tumoral vascularity that is not available on conventional MR imaging (11). Comparisons of rCBV with histologic sections in patients with glioma have demonstrated a significant correlation between tumor vascularity and maximum tumor rCBV (7). Hyperperfused areas of brain tumors were detectable for as small a diameter as 1 cm with high sensitivity (>90%) by using appropriate matrix size (14). DSC perfusion imaging reflects both permeability and perfusion of the tissue and provides accurate measurements of perfusion parameters only if the BBB is intact (15). Measurement of rCBV in consecutive studies is statistically capable of reliably detecting changes >15% between group studies and 25% in individual patients (16). A major drawback of this method is the T1 shortening effect of leaked or recirculated contrast material because of severe BBB breakdown in tumoral tissue, which causes underestimation of CBV value (5).

Comparison of perfusion imaging or postprocessing techniques is beyond the scope of this study. This prospective clinical study was designed to estimate diagnostic accuracy of rCBV measurement in preoperative differentiation and grading of malignant intraaxial solitary brain tumors by using standard DSC T2*-weighted fast field echo (FFE) echoplanar imaging (EPI) during first pass of a bolus injection of contrast material. The main purposes were as follows: (1) to calculate rCBV values for different tumor groups; (2) to estimate a cutoff rCBV value for grading or differentiation; and (3) to find a correlation, if any, between rCBV values and degree of malignancy or tumor type.

Methods

Patient Population

Seventy-five patients with histologically confirmed brain tumor were prospectively evaluated by MR imaging and standard DSC T2*-weighted FFE-EPI during the first pass of a bolus injection of contrast material before the surgical procedure. Patients having more than one lesion or having steroid regimen or chemotherapy before MR examination were excluded from the study. Diagnoses in all patients were histologically confirmed by surgical resection or biopsy because of the location of lesions in vital or eloquent anatomic parts of the brain, and histologic results were used as the reference standard. Informed consent was obtained from all patients for MR examinations and review of patient records and images.

MR Imaging Evaluation

All patients were examined by 1.5T superconducting MR scanner (New Intera Nova; Philips Medical Systems, Best, the Netherlands) by using a standard quadrature head coil with version 9 software release. The system was equipped with magnetic field gradients capable of a maximum strength of 33 mT/m and maximum slew rate of 160 T/m/s. Axial T1-weighted (583/15 ms; 1 excitation) spin-echo (SE), dual T2-weighted (2295/15–90 ms; 2 excitations) SE, and fast fluid-attenuated inversion recovery (FLAIR) (8000/100/2000 ms; 1 excitation) images were obtained by using 5-mm section thickness with 1-mm intersection gap, 220 × 220 mm field of view (FOV), and 256 × 256 matrix size. After the DSC perfusion scans, contrast-enhanced T1-weighted SE images were also obtained in 3 orthogonal planes.

DSC Perfusion Scans

All patients underwent placement of an 18- or 20-gauge intravenous catheter before imaging, usually in the antecubital area, for the purpose of rapid contrast agent administration. We used a susceptibility T2*-weighted multislice multishot FFE-EPI sequence with ProSet (water selective excitation) prepulse. The imaging parameters were as the follows: 627/30 ms TR/TE; 40° flip angle; 1 excitation; 230 × 230 mm FOV; 5–7-mm section thickness; 128 × 128 reconstruction matrix; 1.8 × 3.1 mm measured and 1.8 × 1.8 mm reconstructed voxel size; 0% intersection gap; 1592.1 Hz/pixel signal intensity bandwidth in EPI readout direction; 17 EPI factor; 58% actual scan percentage; and 100% relative signal intensity level. Ten sections were obtained without intersection gap to cover the entire lesion volume identified on T2-weighted images. A series of 50 multisection acquisitions was acquired at 1.9-second intervals, the total acquisition time being 1 minute 37 seconds. The first 10 acquisitions are performed before the contrast agent injection to establish a precontrast baseline. At the eleventh acquisition, 0.2 mmol/kg of body weight of gadodiamid was injected with a power injector (Spectris; Medrad Inc., Indianola, PA) at a rate of 6 mL/s through an 18- or 20-gauge intravenous catheter, immediately followed by a bolus injection of saline at the same rate for a total of 20 mL. Axial contrast-enhanced T1-weighted images were obtained after the perfusion images, by using the same parameters as for the precontrast images.

Postprocessing and CBV Calculation

The DSC perfusion images were transferred to Easy Vision R4 (Philips Medical Systems). Image analysis and CBV measurements were performed with T2* perfusion tool software. The raw data were processed off-line as described elsewhere (2, 5, 17, 18). A 3 × 3 voxel smoothing kernel was applied to all raw images before integration. During the first pass of the bolus of paramagnetic contrast material, the signal intensity in T2*-weighted sequence decreased, whereas the signal intensity partially restored directly after the passage (19). The relative measure of contrast agent concentration can be calculated from signal-intensity changes over time on kinetic principles for nondiffusible tracers by using following relationship: $\Delta R2^*(t) = (-k/\mathrm{TE}\ \ln[St]/S\ [0])$, where TE is the echo-time, k is an unknown proportionality constant, $S(t)$ is the signal intensity at time t, and $S(0)$ is the precontrast signal intensity (3, 5, 17, 20). The contribution of tracer leakage or recirculation due to disruption of BBB in tumoral tissue can be minimized by using a mathematical model (fitting gamma variate function to the measured $\Delta R2^*$ curve) (3, 5, 17, 20). The area under this curve is proportional to the regional CBV (3, 5, 20).

Data Analysis

Three investigators (N.B., M.K., and A.F.), blinded to clinical information, evaluated MR images. They drew all regions of interest with consensus for the rCBV values recording to eliminate interobserver variability. At least 5 uniform regions of interest of 5 pixels had been selected from different areas of tumoral, peritumoral, and normal-appearing mirrored areas showing the greatest visually identifiable CBV values on color maps. The tumoral and peritumoral regions were defined on the basis of the following imaging features: (1) normal tissue—

an area containing no enhancement, normal signal intensity on T2 and FLAIR images; (2) tumoral area—a region containing clearly well-defined solid portion, preferably uniform contrast enhancement, and high signal intensity on T2 and FLAIR images; and (3) peritumoral area—as a region clearly outside of the well-defined solid portion, absolutely containing no enhancement, and high or normal signal intensity on T2 and FLAIR images. To provide the highest intraobserver and interobserver reproducibility in CBV measurements, macroscopic cystic/necrotic areas, CSF-filled sulci or cisterns, and major vessels were avoided (4). The area of regions of interest was kept constant to minimize confounding factors in rCBV analysis (21). The highest CBV value of 5 regions of interest was recorded for each area. Although the calculated CBV from the area under fitted curve was used, this also did not yield an absolute measurement (3). It was necessary to express the measurement relative to standard reference, which was called rCBV (3). All measured CBV values were normalized by dividing the maximum tumoral and peritumoral CBV values by the normal CBV value. The rCBV values obtained from tumoral ($rCBV_T$) and peritumoral ($rCBV_P$) areas were recorded for statistical analysis.

Histopathologic Classification

Specimens obtained from surgical procedures were fixed in formalin and submitted for routine hematoxylin-eosin staining in addition to immunohistochemistry. The presence of pleomorphism, atypia, mitosis, necrosis, astrogliosis, and macrophage infiltration were noted for each patient. For statistical purposes, all glial tumors were categorized as LGGTs (grades I–II) and HGGTs (grades III–IV) by using World Health Organization 2000 classification (22). Pilocytic astrocytomas (PASs) and diffuse astrocytomas (DASs) were classified as LGAs. Anaplastic astrocytomas (AASs) and glioblastomas multiforme (GBMs) were classified as high-grade astrocytomas (HGAs). Low- (LGODGs) and high- (HGODGs) grade oligodendrogliomas were evaluated as nonastrocytic tumors. All kind of metastases (METs) were grouped as MET.

Statistical Analysis

All mean rCBV values were compared among the tumor groups with independent sample *t* test assuming unequal variances for the survival data or one-way analysis of variance (ANOVA) and Tamhane's T2 test assuming unequal variances, where appropriate, to correct for the effect of multiple comparisons, by using SPSS release 11.0 program (SPSS for Windows; SPSS Inc., Chicago, IL). The correlation between different parameters was tested by 2-tailed Pearson correlation coefficients. A stepwise multiple linear regression analysis was used to analyze the relationship of all possible MR imaging findings to $rCBV_T$ and $rCBV_P$ values. The mean difference was significant at the .05 level. The stepwise multiple linear regression and binormal receiver operating characteristic (ROC) analyses were performed to determine optimum thresholds for tumor grading and differentiation. Hence, tumors classified as high grade and found at histologic examination to be high grade were considered true-positive findings; low-grade tumors that were histologically confirmed as low grade were considered true-negative findings. The area under the ROC curve for rCBV ratios, a measure of diagnostic accuracy, was calculated. For each possible cutoff value, which has the highest area under the ROC curve, the sensitivity, specificity, positive predictive value (PPV), negative predictive value (NPV), and accuracy were calculated by using 2×2 contingency table.

Results

Seventy-five cases satisfying the inclusion criteria were examined in this study. Fifty-eight (77.33%) primary and 17 (22.67%) metastatic solitary intraaxial malignant brain tumors, in 45 men and 30 women ranging from 11 to 85 years of age (mean, 39.93 ± 18.33 years), were examined during a 17-month period from August 2003 to December 2004. All DSC T2*-weighted FFE-EPI data were acquired during the conventional MR imaging. In 6 patients, perfusion imaging was repeated because of insufficient diagnostic quality of perfusion data due to severe motion artifacts. Surgical procedure was performed 2–14 days after MR imaging.

Histopathologic Findings

Thirty-six (48.00%) of 75 solitary malignant intraaxial brain tumors were classified as LGGTs, 22 (29.33%) as HGGTs, and 17 (22.67%) as METs (7 breast carcinomas, 4 lung small-cell carcinomas, 3 colon mucinous adenocarcinomas, 2 ovarian adenocarcinomas, and 1 squamous cell carcinoma). The distribution of tumor subgroups and descriptive statistics of mean $rCBV_T$ and $rCBV_P$ values of different tumor groups is presented in Tables 1–3.

Grading

Both $rCBV_T$ and $rCBV_P$ measurements were significantly effective in grading primary glial tumors as LGGT (Fig 1) and HGGT (Fig 2) ($P < .001$). The scatter (Fig 3) and correlation (Fig 4) plots of $rCBV_T$ and $rCBV_P$ values of different tumor groups showed that higher degree of malignancy was linearly correlated with higher $rCBV_T$ and $rCBV_P$ values ($r = 0.768$ and $r = 0.674$; $P < .001$). The $rCBV_T$ cutoff value of 3.9 (Table 4) and the $rCBV_P$ cutoff value of 1.9 (Table 5) could be used with high sensitivity (95.46% and 68.18%, respectively), specificity (91.67% and 100%, respectively), and accuracy (93.10% and 87.93%, respectively).

When astrocytic and nonastrocytic tumors were evaluated separately, rCBV measurement for grading was more effective than evaluating them together. Both $rCBV_T$ and $rCBV_P$ values were statistically effective in grading of astrocytic tumors ($P < .001$). The linear Pearson correlations and degree of malignancy between $rCBV_T$ and $rCBV_P$ values were stronger than those of glial tumors ($r = 0.912$ and $r = 0.719$; $P < .001$). All 24 LGAs (100%) and all 15 HGAs (100%) were correctly classified by using the clear $rCBV_T$ cutoff value of 2.6 (ROC area of 1.000 ± 0.00; $P < .001$) with 100% sensitivity, specificity, and accuracy (Table 4). All HGAs had $rCBV_T$ values >3.15 and all LGAs had $rCBV_T$ values <2.52. The $rCBV_P$ cutoff value of 1.5 was less effective than $rCBV_T$ in the grading of astrocytic tumors.

The $rCBV_T$, but not $rCBV_P$, values were statistically effective in grading of nonastrocytic tumors ($P < .05$). All HGODGs (7/7 [100%]) and 83.33% of LGODGs (10/12) were classified by using the $rCBV_T$ cutoff value of 4.3. The $rCBV_T$ values were linearly correlated with the differentiation of nonastrocytic gliomas ($r = 0.772$; $P < .001$).

The overall diagnostic accuracy of rCBV measure-

TABLE 1: Descriptive statistics of different tumor groups

Tumor Type*	*n* (%)	Parameter	Mean/SD/SE	95% CI for Mean	Range
LGGT (I–II/IV)	36/75 (48.00)	$rCBV_T$	2.30/1.12/0.19	1.92–2.68	0.84–5.73
		$rCBV_P$	1.18/0.24/0.04	1.10–1.26	0.77–1.86
LGAT (I–II/IV)	24/75 (32.00)	$rCBV_T$	1.75/0.38/0.08	1.59–1.91	0.84–2.52
		$rCBV_P$	1.15/0.23/0.05	1.05–1.25	0.77–1.86
LGODG (II/IV)	12/75 (16.00)	$rCBV_T$	3.40/1.29/0.37	2.59–4.22	1.73–5.73
		$rCBV_P$	1.23/0.25/0.07	1.07–1.38	0.87–1.83
HGGT (III–IV/IV)	22/75 (29.33)	$rCBV_T$	5.42/1.52/0.33	4.74–6.09	3.15–8.96
		$rCBV_P$	2.17/0.82/0.18	1.80–2.53	1.00–4.14
HGAT (III–IV/IV)	15/75 (20.00)	$rCBV_T$	4.78/0.99/0.26	4.23–5.33	3.15–6.58
		$rCBV_P$	1.99/0.59/0.15	1.66–2.31	1.00–3.09
HGODG (III/IV)	7/75 (9.33)	$rCBV_T$	6.78/1.63/0.62	5.27–8.29	4.55–8.96
		$rCBV_P$	2.55/1.15/0.43	1.49–3.61	1.23–4.14
MET	17/75 (22.67)	$rCBV_T$	3.21/0.98/0.24	2.70–3.71	1.27–5.60
		$rCBV_P$	0.97/0.09/0.02	0.93–1.02	0.80–1.13

Note.—LGGT indicates low-grade glial tumor; LGAT, low-grade astrocytic tumor; LGODG, low-grade oligodendroglioma; HGGT, high-grade glial tumor; HGAT, high-grade astrocytic tumor; HGODG, high-grade oligodendroglioma; MET, metastasis; $rCBV_T$, tumoral relative cerebral blood volume; $rCBV_P$, peritumoral relative cerebral blood volume.

* Roman numerals in parentheses show tumor grade according to the World Health Organization 2000 classification scheme.

TABLE 2: Descriptive statistics of low-grade astrocytomas

Tumor Type*	*n* (%)	Parameter	Mean/SD/SE	95% CI for Mean	Range
PAS (I/IV)	10/75 (13.33)	$rCBV_T$	1.71/0.45/0.14	1.39–2.03	0.84–2.52
		$rCBV_P$	0.97/0.14/0.05	0.87–1.07	0.77–1.29
DAS (II/IV)	14/75 (18.67)	$rCBV_T$	1.78/0.35/0.09	1.58–1.98	1.29–2.43
		$rCBV_P$	1.28/0.19/0.05	1.17–1.39	1.07–1.86

Note.—PAS indicates pilocytic astrocytoma; DAS, diffuse astrocytoma; $rCBV_T$, tumoral relative cerebral blood volume; $rCBV_P$, peritumoral relative cerebral blood volume.

* Roman numerals in parentheses show tumor grade according to the World Health Organization 2000 classification scheme.

TABLE 3: Descriptive statistics of high-grade astrocytomas

Tumor Type*	*n* (%)	Parameter	Mean/SD/SE	95% CI for Mean	Range
AAS (III/IV)	4/75 (5.33)	$rCBV_T$	4.09/0.06/0.03	3.99–4.19	4.04–4.18
		$rCBV_P$	1.92/0.43/0.22	1.23–2.61	1.28–2.19
GBM (IV/IV)	11/75 (14.67)	$rCBV_T$	5.03/1.05/0.32	4.32–5.74	3.15–6.58
		$rCBV_P$	2.01/0.65/0.20	1.58–2.45	1.00–3.09

Note.—AAS indicates anaplastic astrocytoma; GBM, glioblastoma multiforme; $rCBV_T$, tumoral relative cerebral blood volume; $rCBV_P$, peritumoral relative cerebral blood volume.

* Roman numerals in parentheses show tumor grade according to the World Health Organization 2000 classification scheme.

ments was clearly higher when astrocytic and nonastrocytic tumors were evaluated separately.

Differentiation

The differentiation of METs (Fig 5) from LGGTs and HGGTs was more problematic than grading. The mean differences of $rCBV_T$ ($P < .05$) and $rCBV_P$ ($P < .001$) between LGGTs and METs were statistically significant. METs had higher $rCBV_T$ ($r = 0.372$; $P < .05$) but lesser $rCBV_P$ ($r = -0.433$; $P < .001$) values than LGGT, but these were weaker correlations than those $rCBV_T$ ($r = 0.650$; $P < .001$) and $rCBV_P$ ($r = 0.699$; $P < .001$) values between HGGTs and METs. No clear $rCBV_T$ and $rCBV_P$ cutoff values were detected for exact differentiation (Table 4 and 5). The mean differences of $rCBV_T$ and $rCBV_P$ between HGGTs and METs were statistically significant ($P < .001$). As shown in Tables 4 and 5, though no clear cutoff value was present for exact differentiation of METs from HGGTs, the $rCBV_P$ value was more effective than $rCBV_T$ value in the differentiation.

When nonastrocytic tumors were excluded, the mean difference of $rCBV_T$ between METs and both LGAs and HGAs was statistically significant ($P < .001$). The $rCBV_T$ cutoff values of 2.3 and 3.9 could be used to differentiate the METs from LGAs and HGAs, respectively (Table 4 and 5), but the $rCBV_P$ cutoff values of 1.1 and 1.2 could more accurately differentiate the METs from LGAs and HGAs, respectively.

When only nonastrocytic tumors were evaluated,

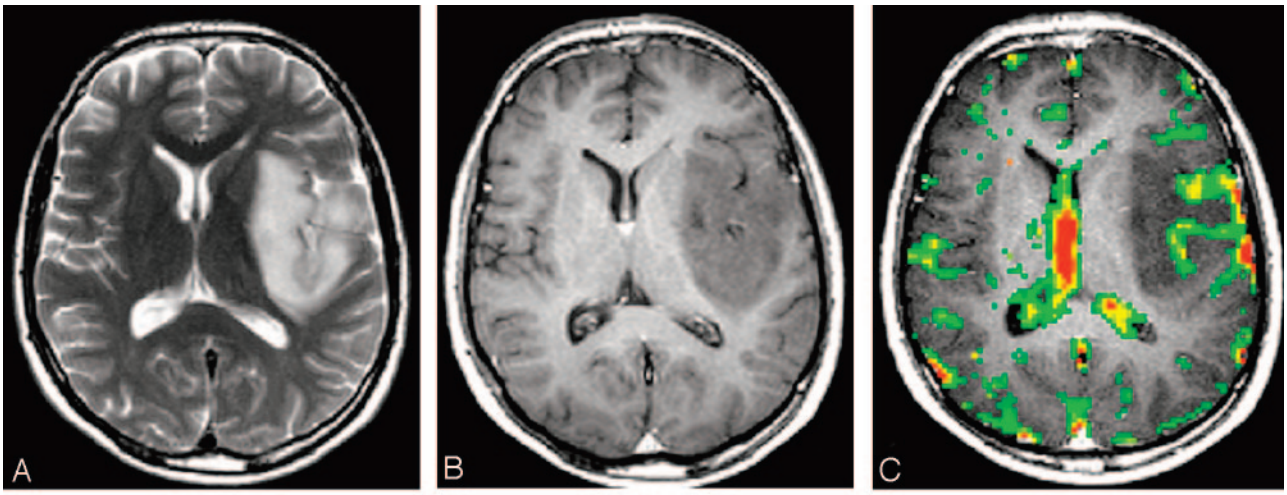

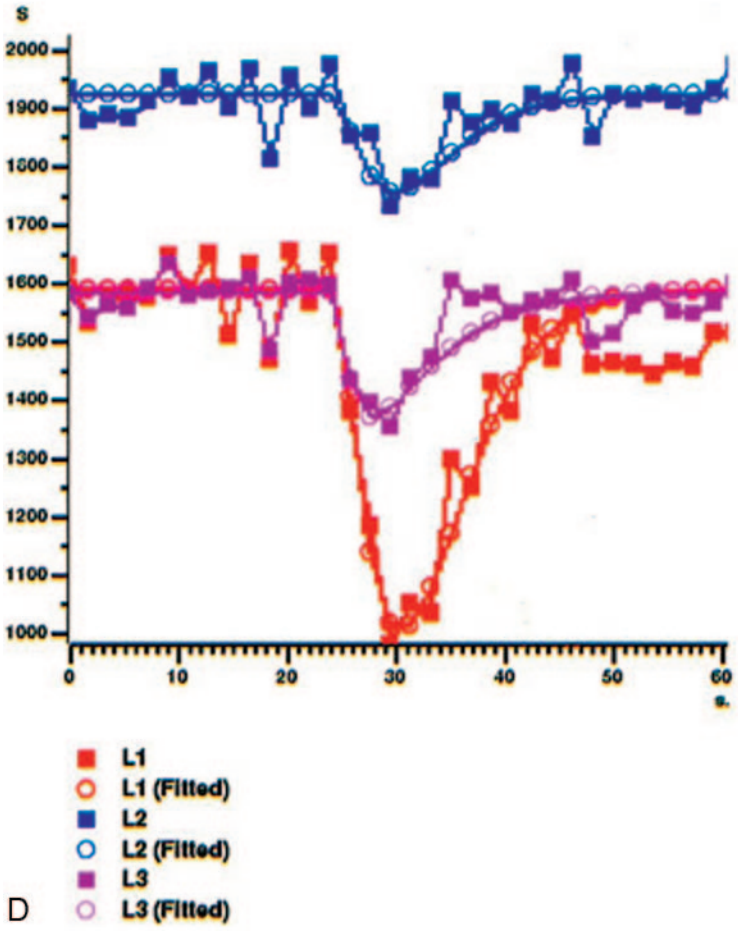

FIG 1. A 22-year-old man with low-grade oligoastocytoma (WHO II) in left frontoparietal lobe.

A, Axial T2-weighted spin-echo image (2295/90) shows hyperintense mass involving left insula and temporal operculum.

B, Tumor does not demonstrate contrast-enhancement on axial T1-weighted image (583/15), which suggests a LGGT.

C, Gradient-echo axial perfusion MR image (627/30) with rCBV color overlay map shows a low $rCBV_T$ value of 1.50 and $rCBV_P$ value of 1.18, in keeping with LGGTs.

D, Time-signal intensity and gamma-variate fitted curves from tumoral (*red*), peritumoral (*blue*), and normal (*purple*) areas show prominent decrease in signal intensity from tumoral area. Decreased signal intensity in peritumoral area is at least equal to that of normal gray matter.

the $rCBV_T$ cutoff value of 3.9, but not $rCBV_P$ values, were significant in the differentiation of HGODGs from METs ($P < .05$; Table 4). Contrary to HGODGs, LGODGs and METs had similar $rCBV_T$ values, but LGODGs had higher $rCBV_P$ values than METs ($P < .05$) and the cutoff value of 1.1 was used for differentiation (Table 5).

When tumoral subtypes having the same grade were compared independently, the results were not much different from total comparison. There were no differences between $rCBV_T$ and $rCBV_P$ values of HGGTs. On the other hand, LGODGs had significantly higher $rCBV_T$, but not $rCBV_P$, values than LGAs, DASs, and PASs ($P < .05$). As shown in Table 4, no clear cutoff values were detected. DASs (Fig 1) had significantly higher $rCBV_P$ values than PASs (Fig 6; $P < .05$), and the $rCBV_P$ cutoff value of 1.1 was used for differentiation (Table 5). This difference was the result of noninfiltrative nature of PASs.

METs had significantly lower $rCBV_T$ values than HGGTs ($P < .05$) and lower $rCBV_P$ values than GBMs ($P < .05$). Although the difference was signif-

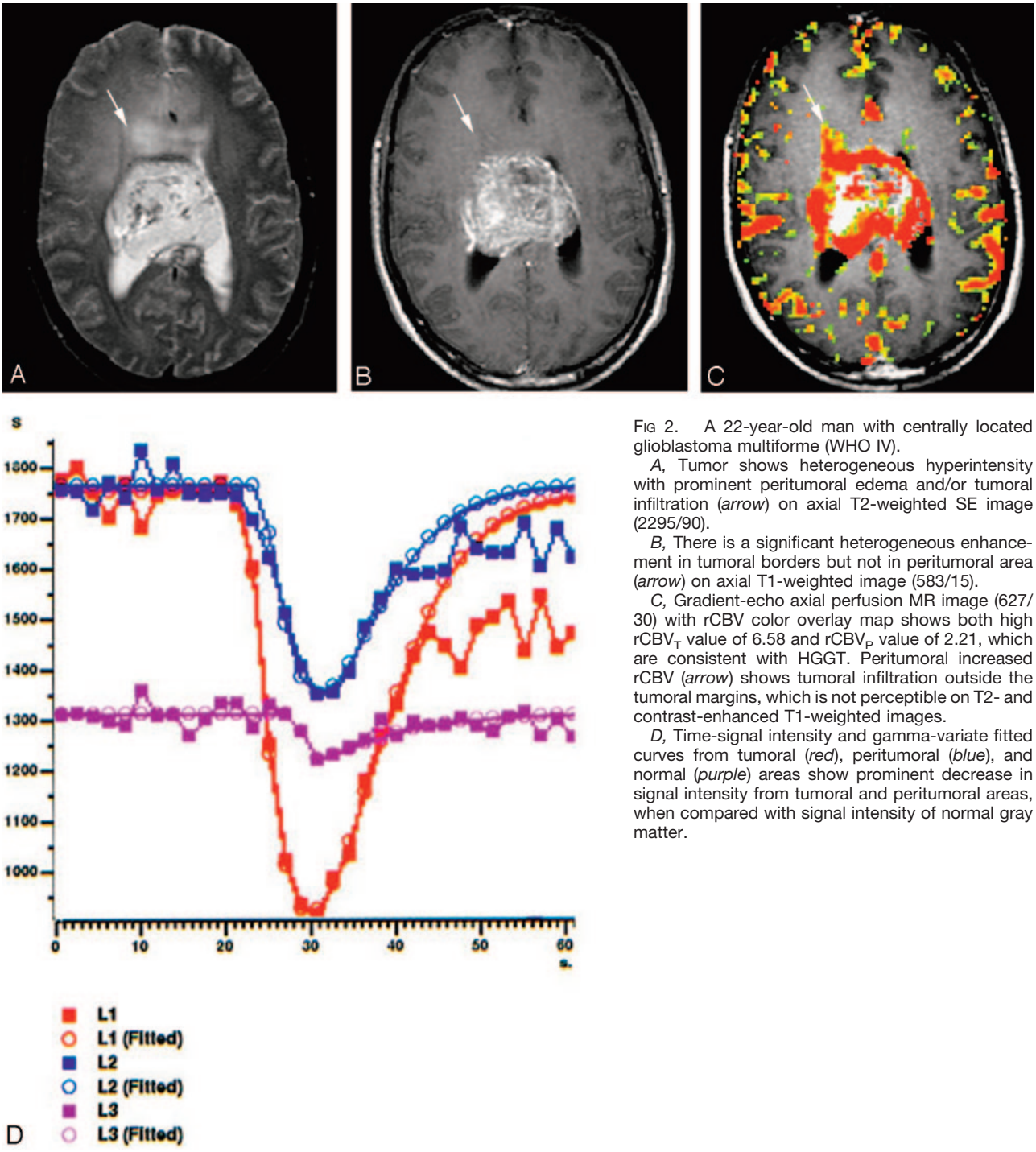

FIG 2. A 22-year-old man with centrally located glioblastoma multiforme (WHO IV).

A, Tumor shows heterogeneous hyperintensity with prominent peritumoral edema and/or tumoral infiltration (*arrow*) on axial T2-weighted SE image (2295/90).

B, There is a significant heterogeneous enhancement in tumoral borders but not in peritumoral area (*arrow*) on axial T1-weighted image (583/15).

C, Gradient-echo axial perfusion MR image (627/30) with rCBV color overlay map shows both high $rCBV_T$ value of 6.58 and $rCBV_P$ value of 2.21, which are consistent with HGGT. Peritumoral increased rCBV (*arrow*) shows tumoral infiltration outside the tumoral margins, which is not perceptible on T2- and contrast-enhanced T1-weighted images.

D, Time-signal intensity and gamma-variate fitted curves from tumoral (*red*), peritumoral (*blue*), and normal (*purple*) areas show prominent decrease in signal intensity from tumoral and peritumoral areas, when compared with signal intensity of normal gray matter.

icant, there was no clear cutoff value to distinguish them from each other (Table 4). The $rCBV_P$ cutoff value of 1.2 was more effective in the differentiation of GBMs from METs (Table 5). The AASs and HGODGs also had higher $rCBV_P$ values than METs; differences were not significant because of insufficient sampling numbers of these tumor groups.

As expected, the METs had significantly higher $rCBV_T$ values than PASs and DASs ($P < .001$). The $rCBV_P$ values of METs were not statistically significant from those of PASs and LGODGs.

Discussion

MR imaging was a novel technique for tumor diagnosis, but it did not have enough efficacy in grading of glial tumors and differentiation of them from METs. MR imaging parameters such as contrast enhancement, mass effect, and signal intensity heterogeneity were correlated with tumor grade; however, these were not strong correlations for exact differentiation or grading. In this study, we tested whether rCBV measurement was effective in grading of glial

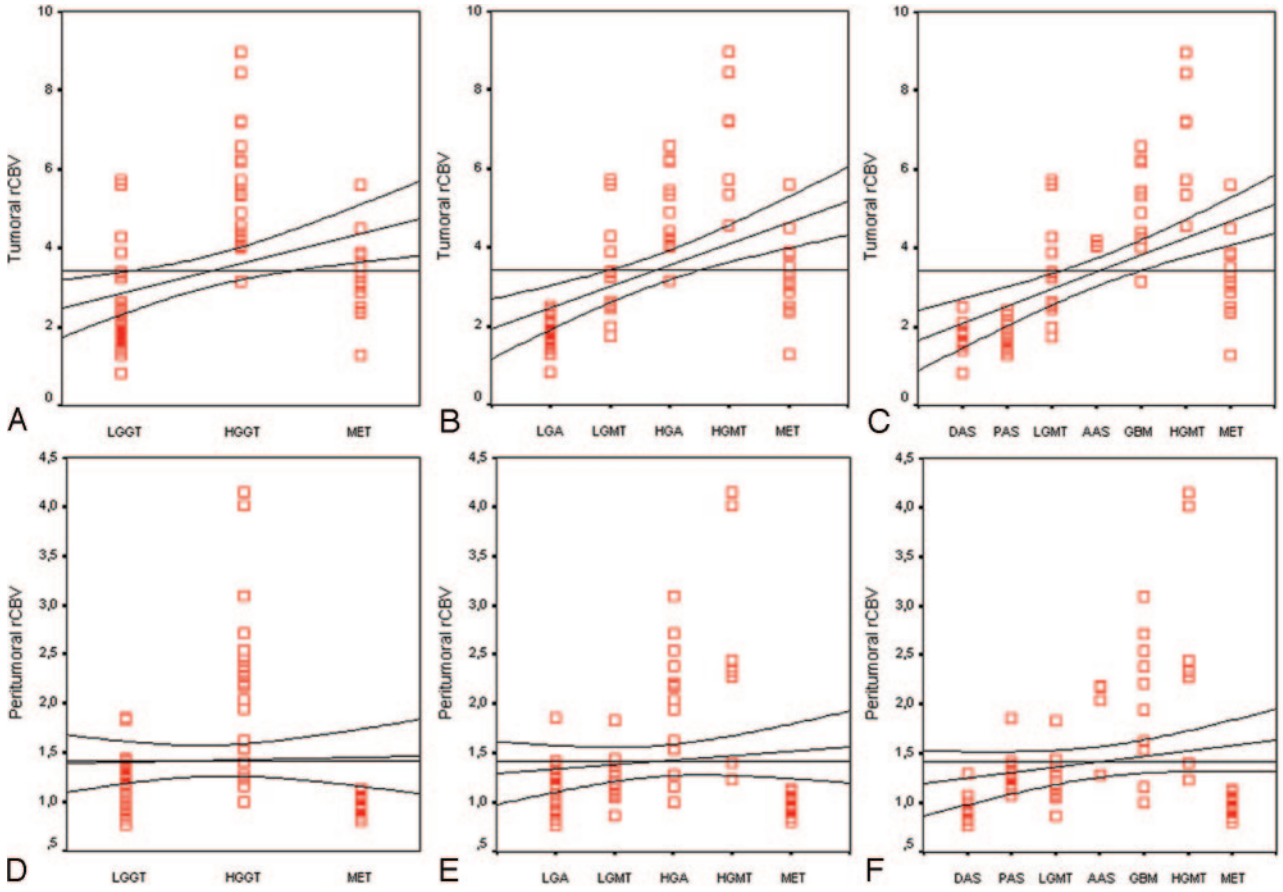

FIG 3. Scatter plots of the tumoral (*A–C*) and peritumoral (*D–E*) rCBV values of different tumor groups show that higher rCBV values are linearly related to higher degree malignancy. Lines are fitted by linear regression with 95% confidence interval. LGGT indicates low-grade glial tumor; HGGT, high-grade glial tumor; MET, metastasis; LGA, low-grade astrocytoma; LGMT, low-grade mixed tumor; HGA, high-grade astrocytoma; HGMT, high-grade mixed tumor; DAS, diffuse astrocytoma; PAS, pilocytic astrocytoma; AAS, anaplastic astrocytoma; GBM, glioblastoma multiforme.

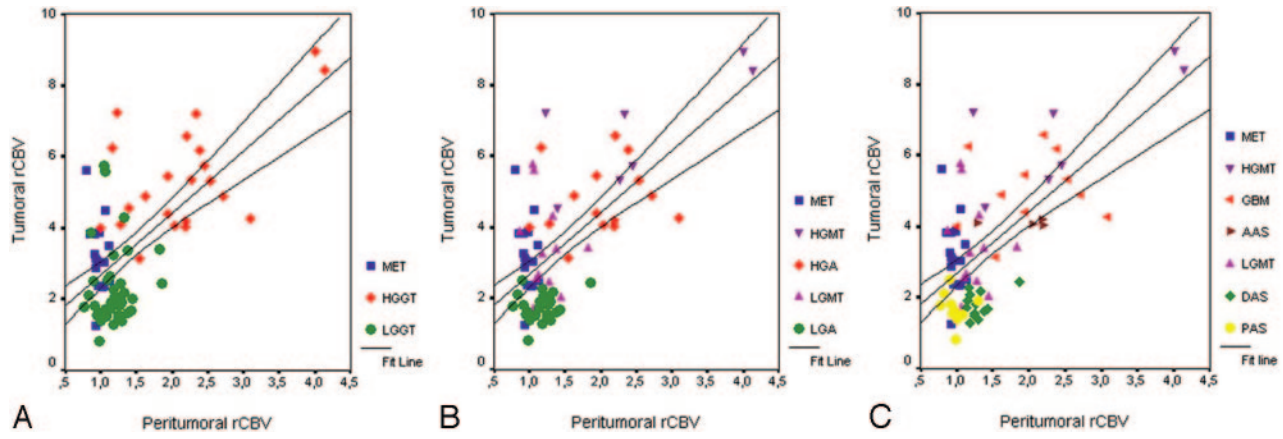

FIG 4. Correlation plots of individual data points show linear correlation between tumoral and peritumoral rCBV values of different tumor groups. Lines are fitted by linear regression with 95% confidence interval.

tumors and differentiation of solitary intra-axial tumors. The specificity and accuracy of the test was more important than its sensitivity, because this was a final diagnostic procedure rather than a screening test.

One of the major findings of this study was that rCBV measurement was more effective than MR imaging parameters in grading of glial tumors. The $rCBV_T$ value of 3.9 and $rCBV_P$ value of 1.9 can accurately classify glial tumors with high sensitivity (95.46% and 68.18%, respectively), specificity (91.67% and 100%, respectively), and accuracy (93.10% and 87.93%, respectively), and both parameters had higher correlation ($r = 0.768$ and $r = 0.674$; $P < .001$) than MR imaging parameters. Our results were comparable with the findings of Law et al (23),

TABLE 4: Statistically significant lowest cutoff $rCBV_T$ values tested for different mean differences

	Cutoff $rCBV_T$ Values														
	For Grading*			For Differentiation†											
Parameter	3.9[a]	2.6[b]	4.3[c]	2.3[d]	3.9[e]	2.3[f]	3.9[g]	3.9[h]	2.2[i]	2.3[j]	3.9[k]	3.9[l]	2.3[m]	2.2[n]	2.5[o]
ROC area	0.936	1.000	0.917	0.804	0.918	0.929	0.908	0.941	0.921	0.935	0.941	0.896	0.875	0.867	0.875
SE	0.037	0.000	0.068	0.061	0.053	0.047	0.060	0.049	0.065	0.052	0.052	0.069	0.072	0.085	0.079
AS	0.000	0.000	0.003	0.000	0.000	0.000	0.000	0.001	0.000	0.000	0.007	0.000	0.000	0.004	0.001
Sensitivity	95.46	100	100	94.12	90.91	94.12	95.46	100	94.12	94.12	100	90.91	83.33	83.33	75.00
Specificity	91.67	100	83.33	66.67	88.24	66.67	88.24	88.24	90.00	92.86	88.24	88.24	91.67	90.00	100
PPV	87.50	100	77.78	57.14	90.91	57.14	91.30	77.78	94.12	94.12	66.67	83.33	83.33	90.91	100
NPV	97.06	100	100	96.00	88.24	96.00	93.75	100	90.00	92.86	100	93.75	91.67	81.82	82.35
Accuracy	93.10	100	89.47	75.47	89.74	75.47	92.31	91.67	92.59	93.55	90.48	89.29	88.89	86.36	88.46

Note.—$rCBV_T$ indicates tumoral relative cerebral blood volume; ROC, area under curve; SE, standard error; AS, asymptotic significance; PPV, positive predictive value; NPV, negative predictive value.

* Superscripts indicate: [a]Low- and high-grade glial tumors; [b]low- and high-grade astrocytic gliomas; [c]low- and high-grade non-astrocytic gliomas.

† Superscripts indicate: [d]Low-grade glial tumors from metastases; [e]high-grade glial tumors from metastases; [f]low-grade astrocytomas from metastases; [g]high-grade astrocytomas from metastases; [h]high-grade non-astrocytic gliomas from metastases; [i]pilocytic astrocytomas from metastases; [j]diffuse astrocytomas from metastases; [k]anaplastic astrocytomas from metastases; [l]glioblastoma multiforme from metastases; [m]low-grade astrocytomas from low-grade oligodendrogliomas; [n]pilocytic astrocytomas from low-grade oligodendrogliomas; [o]diffuse astrocytomas from low-grade oligodendrogliomas.

TABLE 5: Statistically significant lowest cutoff $rCBV_P$ values tested for different mean differences

	Cutoff $rCBV_P$ Values									
	For Grading*		For Differentiation†							
Parameter	1.9[a]	1.5[b]	1.1[c]	1.2[d]	1.1[e]	1.2[f]	1.1[g]	1.2[h]	1.1[i]	1.1[j]
ROC area	0.841	0.879	0.747	0.955	0.733	0.933	0.900	0.909	0.914	0.905
SE	0.063	0.067	0.070	0.037	0.079	0.053	0.066	0.071	0.069	0.061
AS	0.000	0.000	0.004	0.000	0.012	0.000	0.000	0.000	0.001	0.000
Sensitivity	68.18	80.00	61.11	90.91	58.33	86.67	91.67	81.82	92.86	92.86
Specificity	100	95.83	88.24	100	88.24	100	88.24	100	90.00	88.24
PPV	100	92.31	91.67	100	87.50	100	84.62	100	92.86	86.67
NPV	83.72	88.46	51.72	89.47	60.00	89.47	93.75	89.48	90.00	93.75
Accuracy	87.93	89.74	69.81	94.87	70.73	93.75	89.66	92.86	91.67	90.32

Note.—$rCBV_P$ indicates peritumoral relative cerebral blood volume; ROC, area under curve; SE, standard error; AS, asymptotic significance; PPV, positive predictive value; NPV, negative predictive value.

* Superscripts indicate: [a]Low- and high-grade glial tumors; [b]low- and high-grade astrocytic gliomas.

† Superscripts indicate: [c]Low-grade glial tumors from metastases; [d]high-grade glial tumors from metastases; [e]low-grade astrocytomas from metastases; [f]high-grade astrocytomas from metastases; [g]low-grade non-astrocytic glial tumors from metastases; [h]glioblastoma multiforme from metastases; [i]diffuse astrocytomas from pilocytic astrocytomas; [j]diffuse astrocytomas from metastases.

in which they found a cutoff value of 1.75 for rCBV yielded a sensitivity and specificity of 95% and 57.5%, and those of Lev et al (1), in which they found 100% sensitivity and 69% specificity by using a cutoff value of 1.5 for rCBV, as well as the findings of Shin et al (24), in which they found a cutoff value of 2.9 with 91% sensitivity and 83% specificity. Although the sensitivity was similar, our specificity was higher than the others, because we picked up a higher $rCBV_T$ cutoff value (3.9) than the others, to eliminate confounding effects of LGGTs—ie, to minimize type 2 error (number of false-positives).

The higher $rCBV_T$ values of HGGTs mainly reflect increasing vascular proliferation of tumors by increasing grade. The degree of vascular proliferation is one of the most critical criteria in growth and spread of gliomas (22, 25) and in predicting tumor grade and prognosis for several previously well-established reasons (3, 26). The main components of microvascular proliferation in human gliomas—neoangiogenesis and vascular remodeling—are regulated by a set of endothelial cell receptors, which are the main subject of antiangiogenetic therapy (8–11, 22). Typically, these receptors are not expressed in quiescent endothelium but are upregulated in proliferating tumor vessels, in a way that suggests a role in tumor progression (8–11, 22). MR-derived rCBV maps have also correlated with histologic measures of microvessel attenuation from surgical tissue in the evaluation of tumor angiogenesis (27). This high tumoral angiogenesis in human gliomas is always associated with higher microvascular blood volume, which can be effectively measured by DSC perfusion imaging as rCBV value (7, 21, 24, 26–40). Sugahara et al demonstrated a relationship in astrocytic gliomas between the maximum CBV and histologic vascularities that correlated with tumor grade (29). We also found a high linear correlation between $rCBV_T$ values and

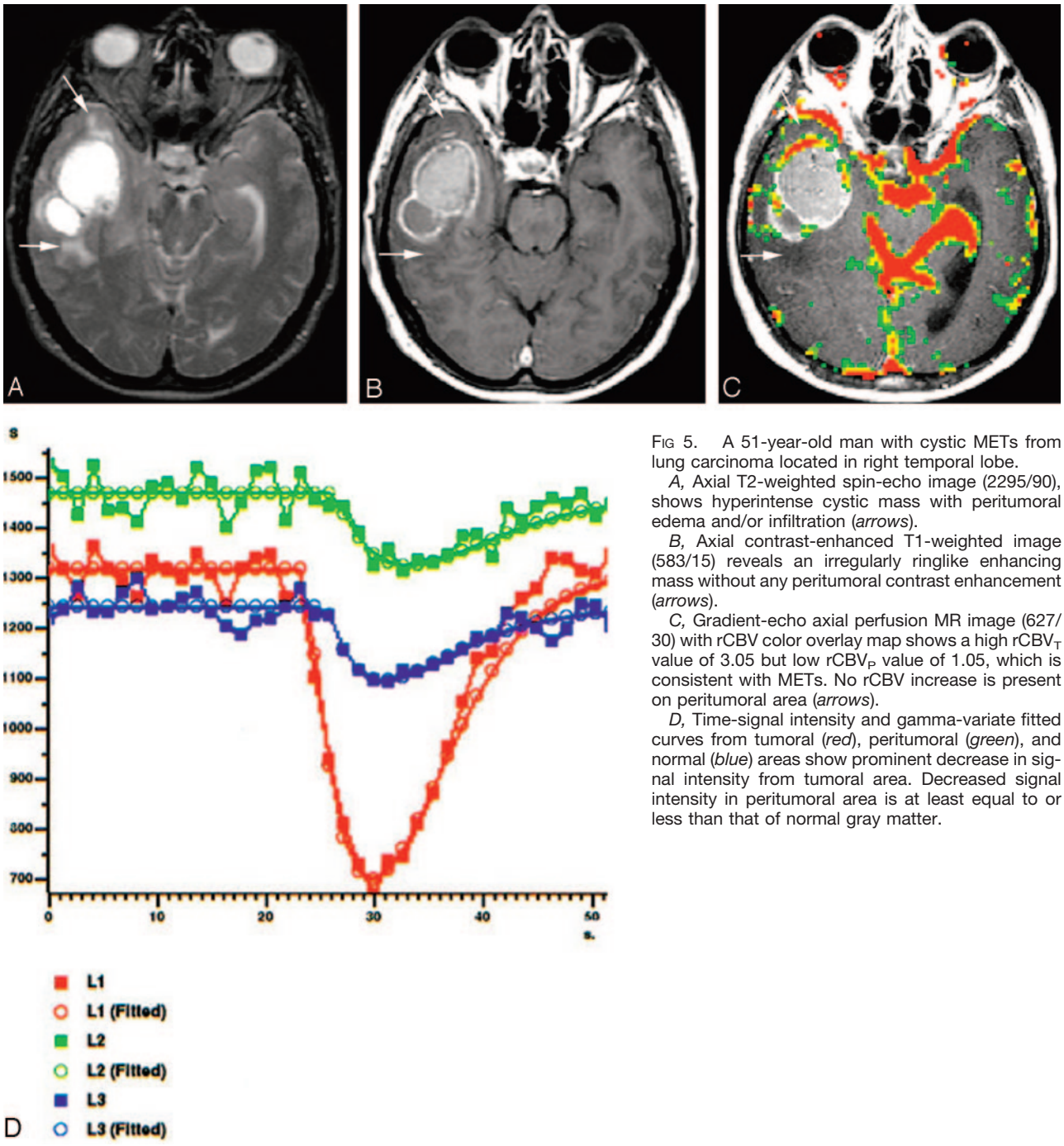

FIG 5. A 51-year-old man with cystic METs from lung carcinoma located in right temporal lobe.

A, Axial T2-weighted spin-echo image (2295/90), shows hyperintense cystic mass with peritumoral edema and/or infiltration (*arrows*).

B, Axial contrast-enhanced T1-weighted image (583/15) reveals an irregularly ringlike enhancing mass without any peritumoral contrast enhancement (*arrows*).

C, Gradient-echo axial perfusion MR image (627/30) with rCBV color overlay map shows a high $rCBV_T$ value of 3.05 but low $rCBV_P$ value of 1.05, which is consistent with METs. No rCBV increase is present on peritumoral area (*arrows*).

D, Time-signal intensity and gamma-variate fitted curves from tumoral (*red*), peritumoral (*green*), and normal (*blue*) areas show prominent decrease in signal intensity from tumoral area. Decreased signal intensity in peritumoral area is at least equal to or less than that of normal gray matter.

tumor grade ($r = 0.768$), but it is not clear whether the increase in rCBV values was due to the dilation of existing vessels, an increase in total number of neocapillaries, or both (26). Furthermore, Daldrup et al (30) have shown a highly positive correlation between tumor permeability to macromolecular contrast medium and tumor grade, but rCBV measurement was a more accurate predictor of tumor grade than vascular permeability (K^{trans}), because tumor regions with high rCBV did not necessarily contain the vessels with highest permeability as in contrast enhancement (28). Disruption of BBB (increased contrast enhancement) and increased vascular permeability can occur before neovascularization, resulting in an increase in tumoral blood volume (26), and increases in both vascular permeability and tumoral blood volume can occur in varying degrees and durations during complex development of human gliomas (28). The rCBV maps are sensitive for only the perfused part of neocapillary formation and measure only functioning capillaries (7). It is expected to find a higher correlation between rCBV values and microvascular attenuation rather than endothelial proliferation itself, which may or may not lead to tube formation of

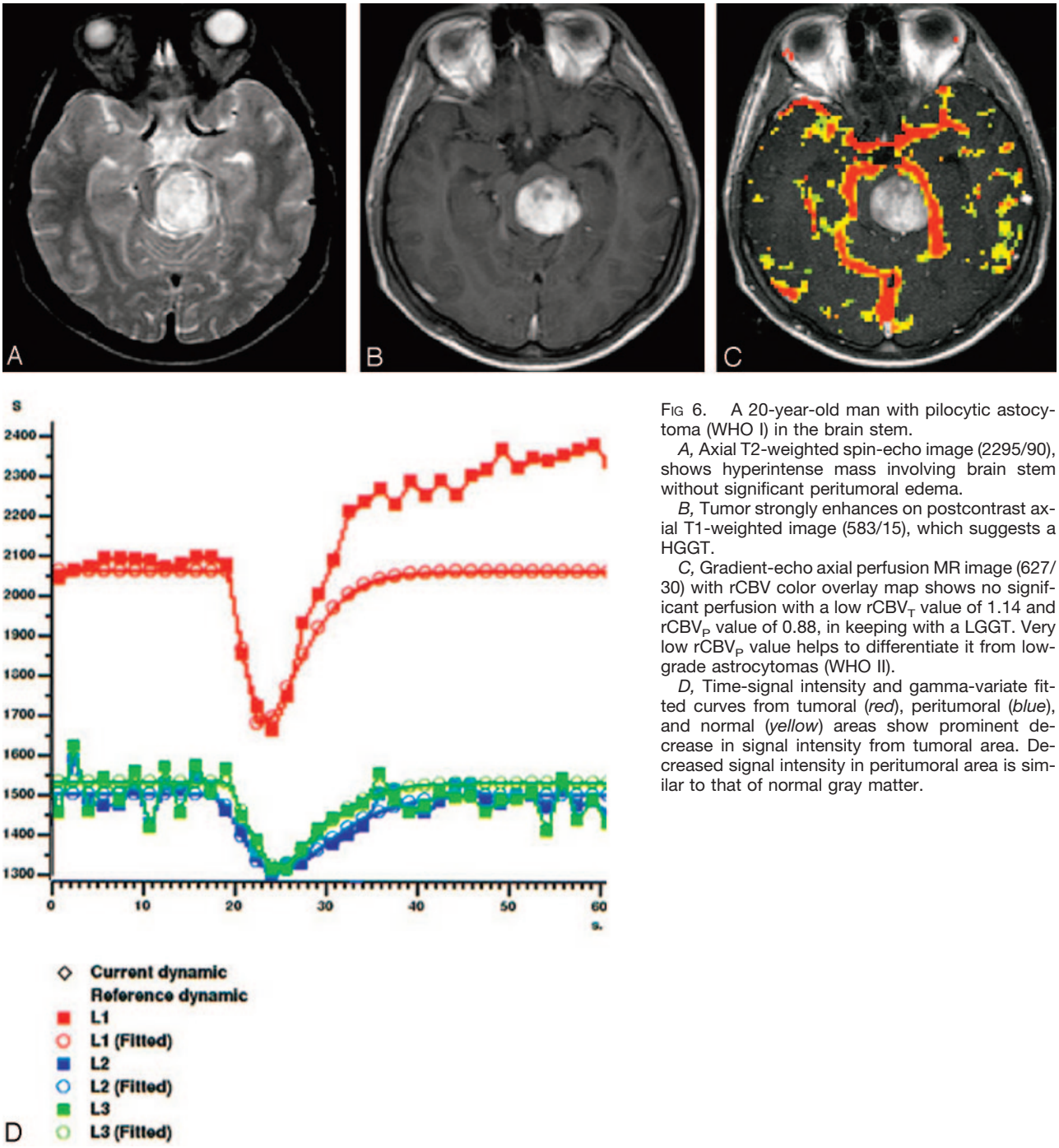

FIG 6. A 20-year-old man with pilocytic astocytoma (WHO I) in the brain stem.

A, Axial T2-weighted spin-echo image (2295/90), shows hyperintense mass involving brain stem without significant peritumoral edema.

B, Tumor strongly enhances on postcontrast axial T1-weighted image (583/15), which suggests a HGGT.

C, Gradient-echo axial perfusion MR image (627/30) with rCBV color overlay map shows no significant perfusion with a low $rCBV_T$ value of 1.14 and $rCBV_P$ value of 0.88, in keeping with a LGGT. Very low $rCBV_P$ value helps to differentiate it from low-grade astrocytomas (WHO II).

D, Time-signal intensity and gamma-variate fitted curves from tumoral (*red*), peritumoral (*blue*), and normal (*yellow*) areas show prominent decrease in signal intensity from tumoral area. Decreased signal intensity in peritumoral area is similar to that of normal gray matter.

functioning capillaries (26). The rCBV measurement is an indirect noninvasive way of approximating functioning part of tumoral angiogenesis, which led us to effective grading of gliomas and differentiation of them from solitary METs.

When nonastrocytic tumors were excluded, the accuracy of $rCBV_T$ measurement was significantly increased, and the clear $rCBV_T$ cutoff value of 2.6 can be used for exact grading with 100% specificity, sensitivity, NPV, PPV, and accuracy. The $rCBV_T$ measurements showed a very strong linear correlation with grading of pure astrocytomas ($r = 0.912$; $P < .001$). Although all HGAs had $rCBV_T$ values >3.15, all LGAs had $rCBV_T$ values <2.52. Although this cutoff value of 2.6 was higher than previously defined cutoff values of 1.5 obtained by using SE-EPI techniques (1, 7) and 1.73 to 2.97 obtained by using GRE-EPI techniques (2, 23, 24, 41), the latter were not clear cutoff values and most of them did not emphasize the difference between the rCBV imaging characteristics of astrocytic and nonastrocytic glial tumors, except 2 of these studies (1, 41). By using SE-EPI technique, Lev et al concluded that glial tumors, which had rCBV values lower than 1.5, did not

contain high-grade components (1). Sugahara et al found that the mean maximum rCBV values of gliomas obtained with GRE-EPI was 1.6-fold higher than those obtained with SE-EPI technique (29). Although SE-EPI was sensitive to microvasculature, the GRE-EPI technique was sensitive to larger vessels, but the latter technique was more useful for grading of glial tumors than the former (21). In our study, the highest $rCBV_T$ values were 2.52 for LGAs and 5.73 for LGODGs. Even if these values were corrected by a coefficient of 1.6 (1.58 and 3.58, respectively), the corrected value for LGODGs was still higher than the previous findings (1). The confounding effect of nonastrocytic glial tumors to glioma grading was well described elsewhere (1, 41). For the most part, we supported these results. Similarly, we also found that the diagnostic accuracy of rCBV measurement was decreased when astrocytic and nonastrocytic tumors were evaluated together, and the correlation of tumoral contrast enhancement was significantly lower in LGODGs than in LGAs. The fine attenuated network of branching capillaries resembling the pattern of chicken wire, which subdivides the tumor into lobules in some cases and increases the tendency for intratumoral hemorrhage, is the major histologic reason for the higher $rCBV_T$ values of LGODGs than those of LGAs. The overlap of rCBV measurements between different glioma grades owing to inherent extreme histologic heterogeneity of gliomas can be minimized and/or eliminated by excluding nonastrocytic gliomas from pure astrocytomas. For this reason, the differentiation of astrocytic and nonastrocytic glial tumors had particular importance. The confounding effect of nonastrocytic gliomas, especially LGODGs, should be remembered in diagnosis for exact glioma grading; on the other hand, the higher rCBV values of LGODGs may be useful in identifying LGGs, which makes them more responsive to PCV (procarbazine, chloroethylnitrosourea, and vincristine) chemotherapy (41). Although there was no clear cutoff value for exact differentiation of LGAs from LGODGs, the $rCBV_T$ cutoff value of 2.3 could be used with high specificity (91.67%) and accuracy (88.89%) to differentiate them. The rCBV maps of gliomas should always be interpreted with MR images, which can provide helpful information for differentiation.

Similarly, $rCBV_P$ values tended to increase with tumor grade, which reflects more diffuse infiltration of adjacent brain structures. Although diffuse infiltration of astrocytomas is largely irrespective of histologic grade, they have an inherent tendency for malignant progression and peritumoral infiltration (22). In our study, increasing $rCBV_P$ values associated with higher tumor grades, which reflected the amount of peritumoral infiltration prominent by tumor grade. This measurement was also helpful for the differentiation of diffusely infiltrating astrocytomas from well-circumscribed PASs. Although DASs usually had higher $rCBV_P$ values than 1.1, PASs had lesser values than this.

The second major finding of our study was that both $rCBV_T$ and $rCBV_P$ values were quite effective in differentiation of METs from both LGGTs and HGGTs. The METs had significantly lesser $rCBV_P$ values than GBMs. Although AASs and HGODGs had also higher $rCBV_P$ values than METs, the number of cases (<10) did not allow us to reach a conclusion. The 1.1 cutoff value of $rCBV_P$ was used for the differentiation. With the exception of small-cell anaplastic tumors and some melanomas, parenchymal METs had histologically well-defined borders with adjacent parenchyma and displaced rather than infiltrated surrounding tissue as they enlarged (22). This was the main explanation of the effectiveness of $rCBV_P$ values in the differentiation of METs from other primary brain tumors. The $rCBV_P$ values of METs (0.97 ± 0.09) were significantly lower than those of both LGGTs (1.18 ± 0.24) and HGGTs (2.17 ± 0.82) ($P < .001$). Our results were similar to the findings of Law et al (42), in which $rCBV_P$ values were 1.31 ± 0.97 and 0.39 ± 0.19 for HGGTs and METs, respectively, and the findings of Chiang et al (43), in which they found $rCBV_P$ values of 2.33 ± 1.61 and 0.84 ± 0.33 for HGGT and METs, respectively. Furthermore, HGGTs (5.42 ± 1.52) had higher $rCBV_T$ values than METs (3.21 ± 0.98) ($P < .001$). This was comparable with the results of Kremer et al (44), in which they found $rCBV_T$ values of 2.61 ± 1.17 and 2.94 ± 0.86 for HGGTs and lung carcinoma METs. They also found that melanoma and renal carcinoma METs had significantly higher $rCBV_T$ values than HGGTs and other METs (44). Our findings showed that METs from lung, breast, colon, ovarian, and squamous carcinomas could be effectively differentiated from LGGTs and HGGTs. Although Kremer et al (44) did not find a statistically significant difference between $rCBV_T$ values of lung carcinoma and HGGTs, in our study the differences between HGGTs and METs was statistically significant ($P < .001$). We did not analyze $rCBV_T$ values of different METs because of insufficient sampling numbers (<10) of each group. The significance of these differences was mainly due to the fact that our metastatic lesions were mainly from lung, breast, colon, ovarian, and squamous carcinomas, which—unlike melanoma or renal carcinoma METs—are not highly vascular.

There were a few potential limitations to our study. One was the heterogeneous sampling numbers of different tumor groups, especially the low sampling numbers of AASs and HGODGs, which prevent more accurately comparison of different tumor types. Another limitation was the lack of measurement of vascular permeability that leads to more accurate comparison of rCBV values for histologic grading and differentiation. The potential pitfall of using T2-gradient echo DSC perfusion imaging was the notable susceptibility from necrosis and hemorrhage, which causes artificial increase or decrease in rCBV measurements. This could be minimized by overlaying colored rCBV maps on contrast-enhanced T1-weighted images with the recognition of necrosis and hemorrhage.

Conclusion

DSC perfusion imaging with rCBV calculation was more effective in the grading of malignant glial brain tumors than in the differentiation of METs from both LGGTs and HGGTs. Although most were not clear ones, we defined multiple statistically significant cutoff values, which can be helpful in daily clinical practice. Among these, only the $rCBV_T$ cutoff value of 2.6 was clear, with 100% sensitivity, specificity, PPV, NPV, and accuracy for grading of pure astrocytomas, mainly due to confounding effect of nonastrocytic gliomas. The $rCBV_T$ values were linearly correlated with degree of malignancy ($r = 0.869$; $P < .001$). The $rCBV_P$ values were more effective than $rCBV_T$ in differentiation of METs from both LGGTs and HGGTs and 1.1 and 1.2 cutoff values of $rCBV_P$ were used for the differentiation. Further studies including larger variances for individual tumor groups are needed to improve the keenness of these cutoff values with higher confidence levels. We believe that combining DSC perfusion imaging with diffusion imaging and proton MR spectroscopy may allow us greater confidence in this context with the penalty of relatively high cost and study time.

References

1. Lev MH, Ozsunar Y, Henson JW, et al. **Glial tumor grading and outcome prediction using dynamic spin-echo MR susceptibility mapping compared with conventional contrast-enhanced MR: confounding effect of elevated rCBV of oligodendrogliomas [corrected].** *AJNR Am J Neuroradiol* 2004;25:214–221
2. Knopp EA, Cha S, Johnson G, et al. **Glial neoplasms: dynamic contrast-enhanced T2*-weighted MR imaging.** *Radiology* 1999;211:791–798
3. Cha S, Knopp EA, Johnson G, et al. **Intracranial mass lesions: dynamic contrast-enhanced susceptibility-weighted echo-planar perfusion MR imaging.** *Radiology* 2002;223:11–29
4. Wetzel SG, Cha S, Johnson G, et al. **Relative cerebral blood volume measurements in intracranial mass lesions: interobserver and intraobserver reproducibility study.** *Radiology* 2002;224:797–803
5. Wong JC, Provenzale JM, Petrella JR. **Perfusion MR imaging of brain neoplasms.** *AJR Am J Roentgenol* 2000;14:1147–1157
6. Su M-Y, Muller A, Lao X, Nalcioglu O. **Tumor characterization with dynamic contrast enhanced MRI using MR contrast agents of various molecular weights.** *Magn Reson Med* 1998;39:259–269
7. Aronen HJ, Gazit IE, Louis DN, et al. **Cerebral blood volume maps of gliomas: comparison with tumor grade and histologic findings.** *Radiology* 1994;191:41–51
8. Brem S, Cotran R, Folkman. J. **Tumor angiogenesis: a quantitative method for histological grading.** *J Natl Cancer Inst* 1972;48:347–356
9. Rampling R, James A, Papanastassiou V. **The present and future management of malignant brain tumours: surgery, radiotherapy, chemotherapy.** *J Neurol Neurosurg Psychiatry* 2004;75(suppl 2):ii24–ii30
10. Leach MO, Brindle KM, Evelhoch JL, et al. **Assessment of antiangiogenic and antivascular therapeutics using MRI: recommendations for appropriate methodology for clinical trials.** *Br J Radiol* 2003;76 (suppl 1):S87–S91
11. Akella NS, Twieg DB, Mikkelsen T, et al. **Assessment of brain tumor angiogenesis inhibitors using perfusion magnetic resonance imaging: quality and analysis results of a phase I trial.** *J Magn Reson Imaging* 2004;20:913–922
12. McKnight TR, von dem Bussche MH, Vigneron DB. **Histopathological validation of a three-dimensional magnetic resonance spectroscopy index as a predictor of tumor presence.** *J Neurosurg* 2002;97:794–802
13. Schwartz RB. **Neuroradiology of brain tumors.** *Neurol Clin* 1995;13:723–756
14. Bitzer M, Klose U, Nägel T, et al. **Echo planar perfusion imaging with high spatial and temporal resolution: methodology and clinical aspects.** *Eur Radiol* 1999;9:221–229
15. Uematsu H, Maeda M, Sadato N, et al. **Vascular permeability: quantitative measurement with double echo dynamic MR imaging: theory and clinical application.** *Radiology* 2000;214:912–917
16. Jackson A, Kassner A, Zhu XP, Li KL. **Reproducibility of T2* blood volume and vascular tortuosity maps in cerebral gliomas.** *J Magn Reson Imaging* 2001;14:510–516
17. Barbier EL, Lamalle L, Décorps M. **Methodology of brain perfusion imaging.** *J Magn Reson Imaging* 2001;13:496–520
18. Weisskoff RM, Rosen BR. **Noninvasive determination of regional cerebral blood flow in rats using dynamic imaging with Gd (DTPA).** *Magn Reson Med* 1992;25:211–212
19. *Intera application guide. Release 9.* Vol 2: *Scan methods.* Best, the Netherlands: Philips Medical Systems;2002:211–217
20. Rosen BR, Belliveau JW, Vevea JM, Brady TJ. **Perfusion imaging with NMR contrast agents.** *Magn Reson Med* 1990;14:249–265
21. Sugahara T, Korogi Y, Kochi M, et al. **Perfusion-sensitive MR imaging of gliomas: comparison between gradient-echo and spin-echo echo-planar imaging techniques.** *AJNR Am J Neuroradiol* 2001;22:1306–1315
22. Kleihues P, Cavenee WK. **WHO Classification of tumours: pathology and genetics of tumours of the nervous system. IARC, Lyon, France,** 2000:9–70
23. Law M, Yang S, Wang H, et al. **Glioma grading: sensitivity, specificity, and predictive values of perfusion MR imaging and proton MR spectroscopic imaging compared with conventional MR imaging.** *AJNR Am J Neuroradiol* 2003;24:1989–1998
24. Shin JH, Lee HK, Kwun BD, et al. **Using relative cerebral blood flow and volume to evaluate the histopathologic grade of cerebral gliomas: preliminary results.** *AJR Am J Roentgenol* 2002;179:783–789
25. Folkman J. **Role of angiogenesis in tumor growth and metastasis.** *Semin Oncol* 2002;29(suppl 16):15–18
26. Cha S, Johnson G, Wadghiri YZ, et al. **Dynamic, contrast-enhanced perfusion MRI in mouse gliomas: correlation with histopathology.** *Magn Reson Med* 2003;49:848–855
27. Pathak AP, Schmainda KM, Ward BD, et al. **MR-derived cerebral blood volume maps: issues regarding histological validation and assessment of tumor angiogenesis.** *Magn Reson Med* 2001;46:735–747
28. Law M, Yang S, Babb JS, et al. **Comparison of cerebral blood volume and vascular permeability from dynamic susceptibility contrast-enhanced perfusion MR imaging with glioma grade.** *AJNR Am J Neuroradiol* 2004;25:746–755
29. Sugahara T, Korogi Y, Kochi M, et al. **Correlation of MR imaging-determined cerebral blood volume maps with histologic and angiographic determination of vascularity of gliomas.** *AJR Am J Roentgenol* 1998;171:1479–1486
30. Daldrup H, Shames DM, Wendland M, et al. **Correlation of dynamic contrast-enhanced magnetic resonance imaging with histologic tumor grade: comparison of macromolecular and small-molecular contrast media.** *Pediatr Radiol* 1998;28:67–78
31. Roberts HC, Roberts TP, Brasch RC, Dillon WP. **Quantitative measurement of microvascular permeability in human brain tumors achieved using dynamic contrast-enhanced MR imaging: correlation with histologic grade.** *AJNR Am J Neuroradiol* 2000;21:891–899
32. Ludemann L, Grieger W, Wurm R, et al. **Comparison of dynamic contrast-enhanced MRI with WHO tumor grading for gliomas.** *Eur Radiol* 2001;11:1231–1241
33. Oh J, Henry RG, Pirzkall A, et al. **Survival analysis in patients with glioblastoma multiforme: predictive value of choline-to-N-acetylaspartate index, apparent diffusion coefficient, and relative cerebral blood volume.** *J Magn Reson Imaging* 2004;19:546–554
34. Lee SJ, Kim JH, Kim YM, et al. **Perfusion MR imaging in gliomas: comparison with histologic tumor grade.** *Korean J Radiol* 2001;2:1–7
35. Aronen HJ, Pardo FS, Kennedy DN, et al. **High microvascular blood volume is associated with high glucose uptake and tumor angiogenesis in human gliomas.** *Clin Cancer Res* 2000;6:2189–2200
36. Roberts HC, Roberts TP, Bollen AW, et al. **Correlation of microvascular permeability derived from dynamic contrast-enhanced MR imaging with histologic grade and tumor labeling index: a study in human brain tumors.** *Acad Radiol* 2001;8:384–391
37. Provenzale JM, Wang GR, Brenner T, et al. **Comparison of permeability in high-grade and low-grade brain tumors using dynamic**

susceptibility contrast MR imaging. *AJR Am J Roentgenol* 2002;178:711–716
38. Roberts HC, Roberts TP, Ley S, et al. **Quantitative estimation of microvascular permeability in human brain tumors: correlation of dynamic Gd-DTPA-enhanced MR imaging with histopathologic grading.** *Acad Radiol* 2002;(suppl 1):S151–S155
39. Schmainda KM, Rand SD, Joseph AM, et al. **Characterization of a first-pass gradient-echo spin-echo method to predict brain tumor grade and angiogenesis.** *AJNR Am J Neuroradiol* 2004;25:1524–1532
40. Tropres I, Lamalle L, Peoc'h M, et al. **In vivo assessment of tumoral angiogenesis.** *Magn Reson Med* 2004;51:533–541
41. Cha S, Tihan T, Crawford F, et al. **Differentiation of low-grade oligodendrogliomas from low-grade astrocytomas by using quantitative blood-volume measurements derived from dynamic susceptibility contrast-enhanced MR imaging.** *AJNR Am J Neuroradiol* 2005;26:266–273
42. Law M, Cha S, Knopp EA, et al. **High-grade gliomas and solitary metastases: differentiation by using perfusion and proton spectroscopic MR imaging.** *Radiology* 2002;222:715–721
43. Chiang IC, Kuo YT, Lu CY, et al. **Distinction between high-grade gliomas and solitary metastases using peritumoral 3-T magnetic resonance spectroscopy, diffusion, and perfusion imagings.** *Neuroradiology* 2004;46:619–627
44. Kremer S, Grand S, Berger F, et al. **Dynamic contrast-enhanced MRI: differentiating melanoma and renal carcinoma metastases from high-grade astrocytomas and other metastases.** *Neuroradiology* 2003;45:44–49